Nanoscale

Journal Name

ARTICLE

The Nanomechanical Signature of Liver Cancer Tissues and Its Molecular Origin†

Mengxin Tian[#a], Yiran Li[#c], Weiren Liu[#a], Lei Jin[a], Xifei Jiang[a], Xinyan Wang[d], Zhenbin Ding[a], Yuanfei Peng[a], Jian Zhou[a,b], Jia Fan[a,b], Yi Cao[*c], Wei Wang[c], Yinghong Shi[*a]

Patients with cirrhosis are at higher risk of developing hepatocellular carcinoma (HCC), the second most frequent cause of cancer-related death. Although HCC diagnosis based on conventional morphological characteristics serves as the "gold standard" in the clinic, there is a high demand for more convenient and effective diagnostic methods that employ new biophysical perspectives. Here, we show that the nanomechanical signature of liver tissue is directly correlated with the development of HCC. Using indentation-type atomic force microscopy (IT-AFM), we demonstrate that the lowest elasticity peak (LEP) in the Young's modulus distribution of surgically removed liver cancer tissues can serve as a mechanical fingerprint to evaluate the malignancy of liver cancer. Cirrhotic tissues shared the same LEP as normal tissues. However, a noticeable downward shift in the LEP was detected when the cirrhotic tissues progressed to a malignant state, making the tumor tissues more prone to microvascular invasion. Cell-level mechanistic studies revealed that the expression level of a Rho-family effector (mDia1) was consistent with the mechanical trend exhibited by the tissue. Our findings indicate that the mechanical profiles of liver cancer tissues directly varied with tumor progression, providing an additional platform for future diagnosis of HCC.

Introduction

As a benign tissue shifts to a metastatic or invasive tumor entity, it undergoes complicated molecular and structural changes in the extracellular matrix (ECM) and cellular scaffold. During this process, mechanical forces influence cellular proliferation, differentiation, migration and tissue development[1, 2]. The mutual interactions between neoplastic cells and their ECM microenvironment are essential determinants of the metastatic process[3]. Therefore, tumorigenesis and tumor progression are accompanied by a progressive loss of biomechanical homeostasis[4] that leads to significant changes in the mechanical phenotypes of both cells and tissues[5].

Over the past two decades, it has become possible to directly characterize changes in the mechanical properties of

a. Department of Liver Surgery, Liver Cancer Institute, Zhongshan Hospital, Fudan University; Key Laboratory of Carcinogenesis and Cancer Invasion of Ministry of Education, Shanghai, China.
b. Institutes of Biomedical Sciences, Fudan University, Shanghai, People's Republic of China.
c. Collaborative Innovation Center of Advanced Microstructures, National Laboratory of Solid State Microstructure and Department of Physics, Nanjing 210093, P.R. China.
d. National Center for Protein Science Shanghai (NCPSS), Institute of Biochemistry and Cell Biology (SIBCB), Shanghai Institutes for Biological Sciences (SIBS), Chinese Academy of Sciences (CAS), Shanghai, China.

# These authors contribute equally to this work.
† Electronic Supplementary Information (ESI) available: [Detailed experimental procedures and Supplementary Figures.]. See DOI: 10.1039/c000000x/

cancer cells and cancer tissues due to the development of a variety of biophysical techniques, such as atomic force microscopy (AFM)[6, 7], magnetic twisting cytometry[8], magnetic tweezers[9] and micropipette aspiration[10]. Cancer cells were revealed to display reduced elastic values compared to normal cells in vitro[7, 11], which may contribute to cancer cell metastasis or recurrence[12, 13]. Similarly, Cross et al. discovered that metastatic cells are softer than benign cells in clinical samples[14]. Investigations of surgically removed tissues may provide information that is more direct and that may be useful for clinical diagnosis. Recently, Plodinec and coworkers used IT-AFM measurements to determine that the elasticity across human breast biopsy samples showed unique mechanical fingerprints that could help define the stages of cancer progression[15]. These findings suggested that cancer progression is accompanied by alterations in nanomechanical properties.

Hepatocarcinogenesis is an intricate multistep process that not only leads to biological and functional alterations but also results in abnormalities in the mechanical and structural characteristics of cells and tissues. However, researchers have primarily focused on the microbiological, metabolic, immunological and pathological aspects of carcinogenesis rather than the mechanical alterations, which might also contribute to pathophysiological outcomes[16, 17]. Therefore, the nanomechanical properties of liver cancer tissues, and especially the intrinsic molecular mechanisms underlying such properties, are largely unknown.

Here, we quantified the Young's moduli of surgically removed samples from HCC patients using IT-AFM with micrometer spatial resolution. This technique allows an investigator to distinguish the mechanical properties of the stiffer extracellular matrix and softer HCC cells in tissue samples. The lowest elasticity peak (LEP), which corresponds to the mechanical signatures of cells, was significantly softer in HCC samples than in normal liver tissues, and it could thus be used as a mechanical fingerprint to evaluate malignancy. Mechanical studies of a stepwise series of metastatic HCC cell lines indicated that there was a correlation between the compliance (softness) of the HCC cells and their invasion and migration potential. At the tissue level, their microscopic vascular invasion capabilities were also associated with tissue compliance. Furthermore, we investigated the molecular mechanism underlying the observed mechanical changes.

Cellular elasticity is heavily influenced by the structure of actin filaments[18], which are regulated by the Rho small GTPase family. Rho activation induces the assembly of contractile actin-myosin filaments (stress fibers), thereby affecting gene expression, cell proliferation and survival[19, 20]. Two major downstream effectors of Rho, mDia (mammalian homolog of Drosophila diaphanous) and ROCK (Rho-associated coiled-coil-forming kinase), play important roles in actin cytoskeleton remodeling. ROCK has been widely investigated[21], and the Rho-ROCK pathway has been strongly implicated in cancer migration and invasion. Our studies revealed that the deregulation of mDia1 and the activation of the ERK1/2 signaling pathway during tumor progression were associated with the softening of cancer cells in the tumor tissues. A tissue microarray of primary tumors from 751 HCC patients confirmed that lower mDia1 expression correlated with poorer prognosis.

Experimental section

Cell culture

An immortalized human liver cell line L02, five HCC cell lines, SMMC7721, Huh7, MHCCL97L, MHCC97H and HCCLM3 and a human hepatic stellate cell LX-2 were used in this study. LX-2 was a gift from Professor Shen XZ[22]. These cell lines were routinely maintained. Except for SMMC7721 that was cultured in 1640 Medium (GIBCO, NY, USA), all other cell lines were cultured in Dulbecco's Modified Eagle Medium (DMEM; GIBCO, NY, USA), supplemented with 10% fetal bovine serum (GIBCO, NY, USA) and 0.1% penicillin/streptomycin (Corning, NY, USA) at 37 °C and 5% CO_2.

Cell Transfection

The mDia1 small interfering RNA (mDia1 siRNA) and the negative control (NC) sequences were purchased from GenePharma (Shanghai, China). The SMMC7721 and Huh7 cell lines were transiently transfected with mDia1 siRNA and NC using the Lipofectamine RNAiMAX transfection reagent (Invitrogen, Carlsbad, CA, USA) according to the manufacturer's instructions. After transfection, the cells were incubated for 48 h before being collected for further analysis. The siRNA sequences are as follows:
mDia1 siRNA1: 5'-GCGAGCAAGUGGAGAAUAUTT-3',
NC sequence: 5'-UUCUCCGAACGUGUCACGUdTdT-3'.

qRT-PCR, Western blotting and Immunofluorescence staining.

RNA extraction, complementary DNA synthesis, quantitative PCR (qRT-PCR) reactions, immunofluorescence staining and western blotting were performed as previously described[23-25].The primers of mDia1, ROCK1, RhoA, RhoB, RhoC and GADPH are show in supplementary table S4. The primary antibodies and dilutions used in western blot were as follows: RhoA, RhoB and RhoC (1:1000, Cell Signaling Technology, Beverly, MA), mDia1 (1:1000; Abcam, Cambridge, UK), ROCK1 (1:500, Santa Cruz, CA, USA), β-actin (1:1000; Sigma, St Louis, MO, USA). For immunofluorescence staining, the cells were incubated with Texas red-conjugated phalloidin (4U/mL; Molecular Probes, Eugene, OR, USA).

Cell Proliferation Assay and Cell Migration Assay

Cell proliferation assay was described previously[25]. Briefly, cells were seeded in a 96-well plate, then CCK-8 solution (Dojindo, Kumamoto, Japan) was added. After incubating for 2 h, the number of viable cells in each well was measured.

Cell migration assay was conducted as previously described[25]. 1×10^5 cells were added to the upper chamber and cultured for 24h in the Transwell chambers (8µm, 24-well format; Corning, NY, USA). Finally, the insert membranes were stained with crystal violet (0.04% in water; 100µL) and cut. Five fields were randomly chosen and counted by Image-Pro Plus v6.0 software (Media Cybernetics, Inc).

Patient samples and Follow-up

Patient samples were described previously[26, 27]. Briefly, 751 specimens were obtained from consecutive patients with HCC who underwent curative resection at the Liver Cancer Institute, Zhongshan Hospital, Fudan University, between 2006 and 2007. The histopathological diagnosis was determined according to the World Health Organization criteria. Tumor differentiation was graded using the Edmondson grading system[28]. Most patients (81.9%) had a hepatitis B virus background, and only 8 patients had hepatitis C virus. The liver function of patients was assessed by the Child-Pugh scoring system. Ethical approval was obtained from the Zhongshan Hospital Research Ethics Committee, and written informed consent was obtained from each patient. Liver fibrosis stage was scored following Kim et al[29]. In brief, Fibrosis was classified into 5 scales: S0, no fibrosis; S1, portal fibrosis without septa; S2, periportal fibrosis and few septa; S3, septal fibrosis; and S4, cirrhosis.

The follow-up data were summarized at the end of December 2012. The follow-up procedures were described in our previous study[30, 31]. Postsurgical patient surveillance was undertaken as previously described[28]. OS was defined as the interval between the dates of surgery and death. TTR was defined as the interval between the dates of surgery and the

ARTICLE

dates of any diagnosed recurrence (intrahepatic recurrence and extrahepatic metastasis). For surviving patients, the data were censored at the date of death or last follow-up.

Tissue microarray and immunohistochemistry

Tissue microarray (TMA) was conducted as previously described[24, 25]. Briefly, all HCC samples were reviewed by histopathologists. Two core biopsies of about 1 mm in diameter were taken from each representative cancerous and peritumoral tissue to construct the TMA slides. Consecutive sections, about 4 μm thick, were placed on 3-aminopropyltriethoxysilane (APTES)-coated slides (Shanghai Biochip Co. Ltd, Shanghai, China).

Immunohistochemical staining was carried out by the avidin-biotin-peroxidase complex method. Briefly, after rehydration and microwave antigen retrieval, monoclonal antibodies against human α-SMA (1:100, DAKO Pharmigen, Glostrup, Denmark), Vimentin (1:100, Abcam, Cambridge, UK), mDia1 (1:50, Abcam, Cambridge, UK), ROCK1 (1:50, Santa Cruz, CA, USA) were applied to the slides, incubated at 4 °C overnight, and followed by the secondary antibody incubation (GK500705, Gene Tech, China) at 37 °C for 1 h. Staining was carried out with DAB and counter-staining with Mayer's hematoxylin. Negative control slides with the absence of primary antibodies were included in all assays.

Scanning electron microscopy (SEM)

The tissue SEM samples were prepared as described by Plodinec et al[15]. In brief, liver tissue samples were stored at 4 °C overnight after fixed in a 2.5% glutaraldehyde aqueous solution. Next, the tissue slices were treated with 2% osmium tetroxide in 0.1 M phosphate-saccharose. Then, the samples were washed by PBS, post-fixed and washed by PBS again. After dehydration in a series of graded ethanol (35-100%), the specimens were dried using a critical point dryer. Finally, the samples were coated with carbon, sputtered with gold palladium and examined with a Hitachi SU8010 scanning electron microscope at an accelerating voltage of 5 kV.

Preparation of Cellular and Tissue samples

The cellular samples were prepared following the procedure described by Lekka et al[32]. Before AFM measurements, L02, HCC cell lines, and LX-2 cells were cultured in the DMEM on the glass coverslips fixed on the Petri dish bottom (Corning, 30 mm). When the semi-confluent monolayer was observed, the coverslips with cells were washed with PBS buffer and mounted on the AFM scanner and measured within the next 1h (at room temperature and ambient conditions, cells preserved their viability).

Human liver tissues were collected from patients received curative liver resection, in the Department of Liver surgery, Zhongshan Hospital of Fudan University. The tissue samples were prepared as described by Plodinec et al[15]. Every case of liver tissue could be divided into two regions, tumor and peritumor. Five cylindrical tissue samples were obtained by using 18G needles from the neoplastic or paraneoplastic

region, respectively. One was used for the IT-AFM measurement and the others for pathological diagnosis or IHC analysis. All tissue slices were preserved in DMEM supplemented with a protease inhibitor cocktail (Complete, Boehringer Mannheim; 1 tablet per 10 mL) without FBS medium and stored at 4 °C to avoid tissue degradation. Before proceeding to AFM, the cylindrical liver specimen (~ 15-20 mm in length and ~ 2 mm in diameter) was rinsed by PBS buffer and then directly glued onto a clean glass slide using a droplet of cyanoacrylate adhesive (0.5μL, AXIA, Kitta, Korea) without further slicing. After gluing for about 15 s, the sample was immediately immersed in PBS and AFM measurements were performed within the next 1-2 h at room temperature.

AFM measurement

AFM experiments were carried out on a commercial AFM (JPK, Nanowizard II, Berlin, Germany). The force curves were obtained by the commercial software from JPK and analysed by a custom written procedure based on Igor pro 6.12 (Wavemetrics Inc). Silicon nitride D cantilevers (MLCT Bruker Company with the half-open angle of the pyramidal face of θ ~20°, tip radius: 20 nm，frequency in air: 15kHz) were used in all experiments. The spring constant of the cantilevers, calibrated by thermal fluctuation method, were in the range of 0.03~0.05 N m^{-1}. The maximum loading force was set at 2-3 nN for tissue sample and 0.8 nN for cell. We chose such indentation force in order to avoid cell death in the experiments while ensure to obtain relatively large data range for fitting. Typically, cells can survive in such nano-indentation experiments as evidenced by the following facts: 1) The cells remain the same shape before and after indentation experiments. 2) All cells remain adhered to the petri dish after the indentation measurement. The dead cells typically cannot remain attached on the petri dish and will go to the suspension (see fig. S12). Actually, sharp cantilever tips have been widely used to manipulate cells. Previous literature reported that the indentation force we used for cell sample is unlikely to penetrate cells and cause cell death.

All AFM experiments were carried out under room temperature. In a typical experiment, the cantilever was moved above the tissue with the help of an optical microscope. The cantilever was brought to the tissue with the constant speed of 3 μm s^{-1}, and held on the tissue surface at constant force of 2-3 nN. Then the cantilever was retracted and moved to another spot for the next cycle. For cell samples, also the cantilever was moved above the centre of a single cell first. Next the cantilever was brought to the cell with the same speed as mentioned above with a constant force of 0.8 nN to the cell surface. Once the force on the cantilever reaches the set point, the piezo will retract immediately. We set a spiral pattern and tested 100 spots on that route (Fig. S15). The indentation fit was done using a custom-written program in Igor and manually checked after the fitting was done. Typically more than 95% of the curves can be fitted nicely (R^2 values of fitting are in the range of 0.68-0.98). The rest 5% curves cannot be fitted automatically using this program because of

the quality of the data were not good. These curves were then fitted manually. We fitted each approaching force-deformation curve in the range of 1 μm from the contact point or the maximum indentation depth to the contact point if the maximum indentation depth is less than1 μm. We chose constant data range for indentation depth to minimize the bias from fitting and the data in this range can be fitted reasonably. By fitting the approaching curve to the Hertz model (1), we can obtained the Young's modulus of the tissue and cell samples. After analysing each force curve, we can get the Young's modulus of the corresponding spot and obtain the 2-D elasticity map. Typically, 3-10 such regions (10μm × 10μm, 100 pixels) were randomly selected on each sample to make the elasticity histogram. In practice, the surface of the tissue sample is relatively rough and the height can vary in a range of a few micrometres, making the measurement among a large area very difficult.

$$F(h) = \frac{2}{\pi} \tan \alpha \frac{E_{sample}}{1 - v_{sample}^2} h^2 \qquad (1)$$

Where F is the stress of the cantilever, h is the depth of the tissue pressed by cantilever tip, α is the half angle of the tip, E is the Young's modulus of the tissue and v is the Poisson ratio. We chose v=0.5 in our calculation.

Statistics

All individual elastic values for a specimen were summarized in Igor pro 6.12 to obtain the distribution of elastic values. Counts were normalized according to the total amount of measured elasticity values per specimen. For data fitting, peaks were located with the multi-peak fitting application of Igor pro. Subsequently, a multi-peak fit was applied to the elasticity distribution. All data are given as mean ± standard deviation. The statistical significance of differences in mean values was assessed with the paired Student's t-test in OriginPro 8.5. Other statistical analyses were performed with SPSS 19.0 for windows (SPSS Inc., Chicago, IL). The Pearson χ^2 test or Fisher's exact test was used to compare qualitative variables; and quantitative variables were analyzed by the *t* test or Pearson's correlation test. Kaplan-Meier analysis was used to determine the survival, survival curves between different groups were calculated with log-rank test. Statistical significance was set at P ≤ 0.05.

Results

Nanomechanical signatures of human liver tissues

To explore the nanomechanical properties of human liver cancer, 40 human specimens (7 normal liver, 14 cirrhotic liver, 13 primary liver cancer, 2 recurrent liver cancer, 2 renal cell carcinoma, 1 esophageal cancer and 1 colon cancer) were obtained from surgery and were systematically studied using IT-AFM in phosphate-buffered saline (PBS). As shown in Fig. 1A, tissue samples carefully collected using 18G needles (~2

mm thick) were glued to a flat glass coverslip for nano-indentation measurement. An optical image obtained under the experimental conditions is shown in Fig. S1. The cantilever was brought into contact with the tissue surface and inserted at a constant speed of 3 μm s-1 until the contact force reached ~2-4 nN (black traces, Fig. 1B). The cantilever was then retracted at the same speed (gray traces, Fig. 1B). The elasticity of the tissue at a given position can be extrapolated by fitting the approaching traces using the Hertz model (red lines, Fig. 1B). Several excellent papers have highlighted the effect of indentation depth on the measured elasticity using Hertz model[33, 34]. In our experiments, we control the indentation force instead of indentation depth. For tissue samples, the indentation force was set to 2-3 nN, and for cell samples, it was set to 0.8 nN. The corresponding indentation depth is ~ 150 nm - 2 μm and 0.3-0.5 μm, respectively, depending of the elasticity of the samples. To minimize the errors from Hertz model fitting, we always chose to fit the 1 μm region from the contact point. In such a practice, different indention depth does not affect our data analysis too much. Because Hertz model was deduced based on elastic solids, deeper indentation depth may make the deformation inelastic and fitting to this region will make the measured Young's moduli bigger than the real value. To figure out the pulling speed effects on elasticity hardening, we tested two different pulling speed experiments on the same cell. The results showed that the lower the speed to 2 μm/s could lead to the decrease of the stiffness by 5% (Fig. S13). However, further decrease of the indentation speed will lead to the drift of the cantilever more significant, which makes the data unreliable (It takes ~10 s for one indentation cycle and ~ 3 h for a tissue sample at an indentation speed of 1 μm/s.). Representative elasticity maps (10 ×10 pixels) of neoplastic (cancer) and paraneoplastic (normal) tissues from a single HCC patient are shown in Fig. 1C-D (top panels) and Fig. S14A. The nanomechanical properties of the tissues based on 3~10 areas (10 μm × 10 μm, 100 pixels) for each tissue are summarized in Figure 1C-D (middle panel). Two clearly distinguishable peaks were observed for both cancerous and paratumoral tissues (Fig. 1C-D, middle panels). The lower (lowest) elasticity peak (LEP) and the higher elasticity peak (HEP) were attributed to the nanomechanical properties of the cancer cells and the ECM, respectively, in accord with the literature[15]. The HEP of ~ 2 kPa for paraneoplastic tissues might be related to chronic hepatitis B virus (HBV), as suggested by subsequent hematoxylin and eosin (HE) staining of sections (Fig. 1C-D, bottom panel). The positions of the HEPs were very scattered, and thus they cannot be used as unique mechanical signatures for diagnosis. However, the LEP distribution in the paraneoplastic tissues was centered at 1.10 ± 0.20 kPa, which was stiffer than the LEP for the neoplastic tissues (0.42 ± 0.17 kPa) (Fig. 1C-D, middle panel). Moreover, based on the results of 15 sample pairs from HCC patients, the difference between the LEPs of neoplastic and paraneoplastic tissues was significant (p < 0.0001) (Fig. 1E). The shift in the LEP was most likely due to substantial changes in cellular shape and

structure, as suggested by histopathology (Fig. 1C-D, bottom panel).

We also measured the elasticity across other types of cancers to examine whether different types of cancers had similar nanomechanical characteristics. Representative elasticity maps and corresponding elasticity distributions are shown in Fig. S2A-D (top and middle panels) and Fig. S14B. Our results show that the elasticity distributions of esophageal and clear cell renal cell carcinoma were more complex; both cancers showed 4 peaks, with LEPs centered at 0.65 and 0.51 kPa, respectively (Fig. S2A-B, middle). HE staining demonstrated that the cancerous cells were buried in the abundant ECM (Fig. S2A-B, bottom). However, there were two peaks in the colon cancer sample and a single peak in the papillary renal cell carcinoma sample (Fig. S2C-D). The absence of HEPs was consistent with the presence of less ECM, as observed in the subsequent HE analysis. Interestingly, although their specific nanomechanical characteristics and tissue structures were diverse, all four types of cancer tissues exhibited similar LEPs (0.33 to 0.65 kPa). Despite the diverse mechanical properties of the ECM, the LEP could be used as a unique mechanical measurement to distinguish normal and cancerous tissues.

Changes in nanomechanical properties during liver cancer progression

Next, we explored whether nanomechanical properties could be used as a signature to monitor liver cancer progression. It has been well established that cirrhosis can lead to HCC. Approximately 1% to 3% of patients diagnosed with cirrhosis will develop HCC annually[35]. Cirrhosis results from necroinflammation and fibrogenesis. Histologically, it is characterized by diffuse nodular regeneration surrounded by dense fibrotic septa with subsequent parenchymal extinction and the collapse of liver structures[36]. Therefore, liver tissues may experience dramatic changes in their nanomechanical properties at different stages during the progression from normal liver to HCC or recurrent HCC.

The elasticity distribution of normal samples mainly exhibited a unimodal trend, with the LEP centered between 0.91 and 1.55 kPa (Fig. 2A-B, left; Fig. S3; Table S1; Fig. S14C); this distribution is characteristic of healthy tissues. HE and Masson's trichrome (Tri. Masson) staining demonstrated that the tissues were well organized, with packed hepatocytes and less fibroconnective tissue (Fig. 2C, left). In normal liver tissues, the portal area is a component of the hepatic lobe, with 4 vessels lying in a meshwork of fibroconnective tissue. In some of the samples, we observed an extremely disordered distribution of elasticity values, with 5 peaks centered from 4.65 to 11.50 kPa (Fig. S3, left); these peaks were attributed to the nanomechanical properties of the portal area (Fig. S4, circled area, right). To further confirm this conjecture, we chose LX-2 cells as the cellular control, which represent a type

of hepatic stellate cell with secreted collagen, and measured their mechanical properties using IT-AFM. The histogram of the Young's moduli for the LX-2 cells exhibited a heterogeneous distribution, with 4 peaks centering at 0.51, 2.18, 3.70 and 7.51 kPa (Fig. S5); this finding is in agreement with the nanomechanics of the portal area. Moreover, this result is also consistent with the elasticity of the highly fibrotic content in benign fibroadenomas (3.68 ± 1.92 kPa)[15].

Due to the turbulence of the intrahepatic scaffold, the elasticity distribution of cirrhotic liver tissues showed two or more peaks. However, the LEPs showed no significant differences compared with normal tissues. The elasticity of the HEP was increased and its distribution was broadened when local fibrogenesis became severe (Fig. 2A-B, liver cirrhosis column). The elasticity of several tissues reached as high as 16 kPa due to the presence of abundant ECM inside the paraneoplastic tissue (Fig. S6). Tri.Masson staining demonstrated the proliferation of ECM distributed around hepatocytes inside the tissue (Fig. 2C); these findings were further confirmed by subsequent SEM analysis (Fig. 2D, at the bottom of liver cirrhosis). It is widely acknowledged that chronic hepatic fibrosis is a driving force behind liver cancer. Thus, the disordered homeostasis of the mechanical microenvironment may contribute to malignant transformation. However, we did not observe obvious changes in the mechanical properties of cancer cells in cirrhotic liver tissues. Therefore, exploration of the link between the mechanical properties of the ECM and carcinogenesis requires additional study.

The elasticity distribution of HCC cancer tissues typically showed two well-separated peaks that were centered at 0.6 and 2.1 kPa (Fig. 2A-B, HCC column; Fig. S7; Table S1). The LEP was significantly decreased compared to cirrhotic and normal liver tissues, thus representing a clear signature for progression to the malignant state. The origin of these mechanical features was revealed by Tri.Masson staining of sections and subsequent SEM: the decreased tumor stroma and changes in the mechanical phenotype of tumor cells make the HCC softer than most other malignant epithelial neoplasms (Fig. 2C-D, HCC column).

We also studied the nanomechanics of recurrent cancer. AFM analysis revealed that the elasticity histogram of recurrent HCC displayed a unimodal peak (Fig. 2A-B, recurrent HCC column; Fig. S8) centered at ~0.45kPa (Table S1), similar to the LEP of HCC. SEM showed that there were more abundant microvillus-like protrusions on the surface of recurrent cancer cells (Fig. 2D; recurrent HCC column). Although curative resection improves the survival of patients, the high recurrence rate is a major obstacle after surgery[37]. Based on limited recurrent HCC samples, it seems that the nanomechanical properties of the tumor might undergo a change during cancer progression, which could serve as a clear signature for the recurrence of HCC.
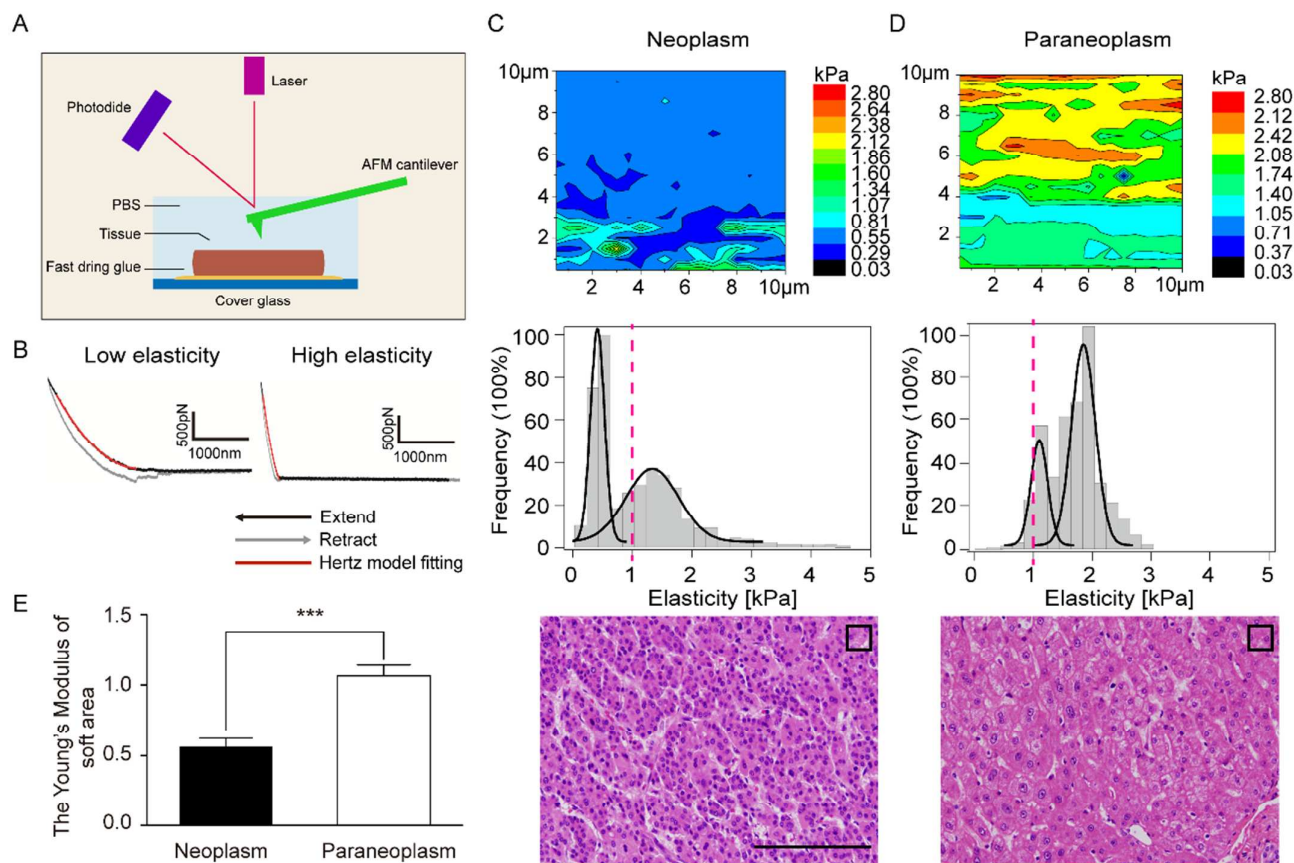
Figure 1. The nanomechanical properties of human liver tissues. A, Schematic illustration of the IT-AFM experiments on liver tissue samples. A freshly obtained tissue sample was glued onto a glass coverslip and immersed in the PBS buffer for the AFM measurement. The cantilever tip was reversely pushed into the tissue sample and retracted to obtain the force-distance trace on each spot, based on which the elasticity can be deduced using Hertz model. B, Representative force-distance traces on spots showing low elasticity (left) and high elasticity (right), respectively. The hysteresis between "extend" and "retract" traces is due to sample deformation and the adhesion between the cantilever tip and the sample. Red line corresponds to the fitting of the contact region in the "extend" trace using Hertz model. C, Mechanical features of the neoplasm. Top: A representative elasticity map (10 μm × 10 μm, 100 pixels) on the HCC tumor tissue. Middle: The elasticity distribution of the HCC tumor tissue based on ~10 randomly selected areas as shown above. Bottom: Hematoxylin and eosin stain (HE stain) of the HCC tumor tissue sample. A dark square (10 μm × 10 μm, 100 pixels) represents the size of elasticity map. Scalebar: 50 μm. D, Mechanical features of the paraneoplasm. The layouts are arranged in the same way as those in Fig. 1C. E, Comparison of the Young's moduli for the neoplastic and paraneoplastic tissues, Student's t test, *** P<0.0001.
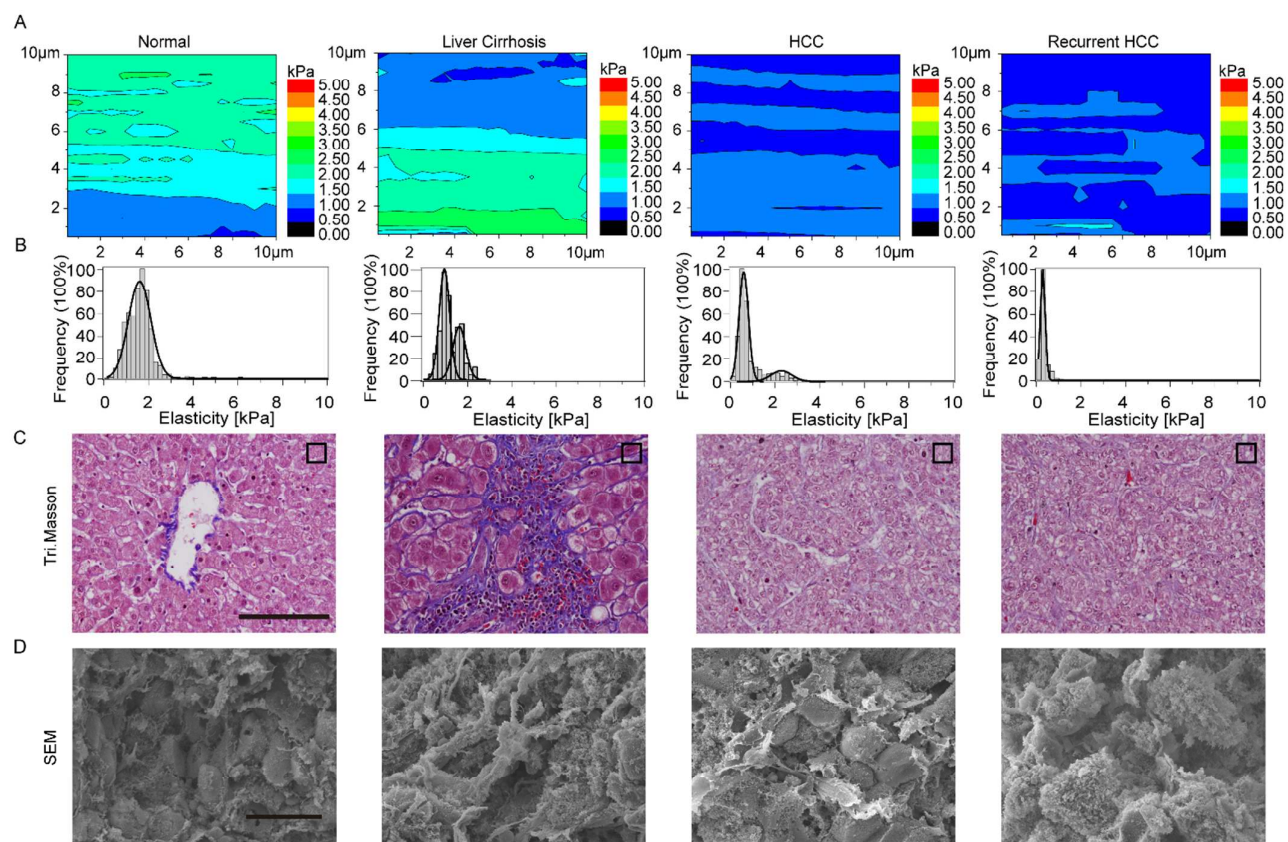
Journal Name

ARTICLE

Figure 2. Changes in nanomechanical properties during liver cancer progression. A-D, Elasticity maps (10 μm × 10 μm, 100 pixels), elasticity distributions, Tri. Masson staining images and SEM images of liver cancer tissues at different stages. From left to right: Normal, liver cirrhosis, HCC and recurrent HCC, respectively. A dark square (10 μm × 10 μm, 100 pixels) represents the size of elasticity map in Tri. Masson staining. Scale bars in Tri. Masson staining and SEM images are both 50 μm. Continuous elasticity maps (10μm × 10μm) was indicative of the softening phenomenon with the progression of liver cancer (left to right). Clearly, the LEP was significantly decreased in the HCC and recurrent HCC tissues as compared with the cirrhotic and normal liver tissues, which is a clear signature for the progression to malignant entity.
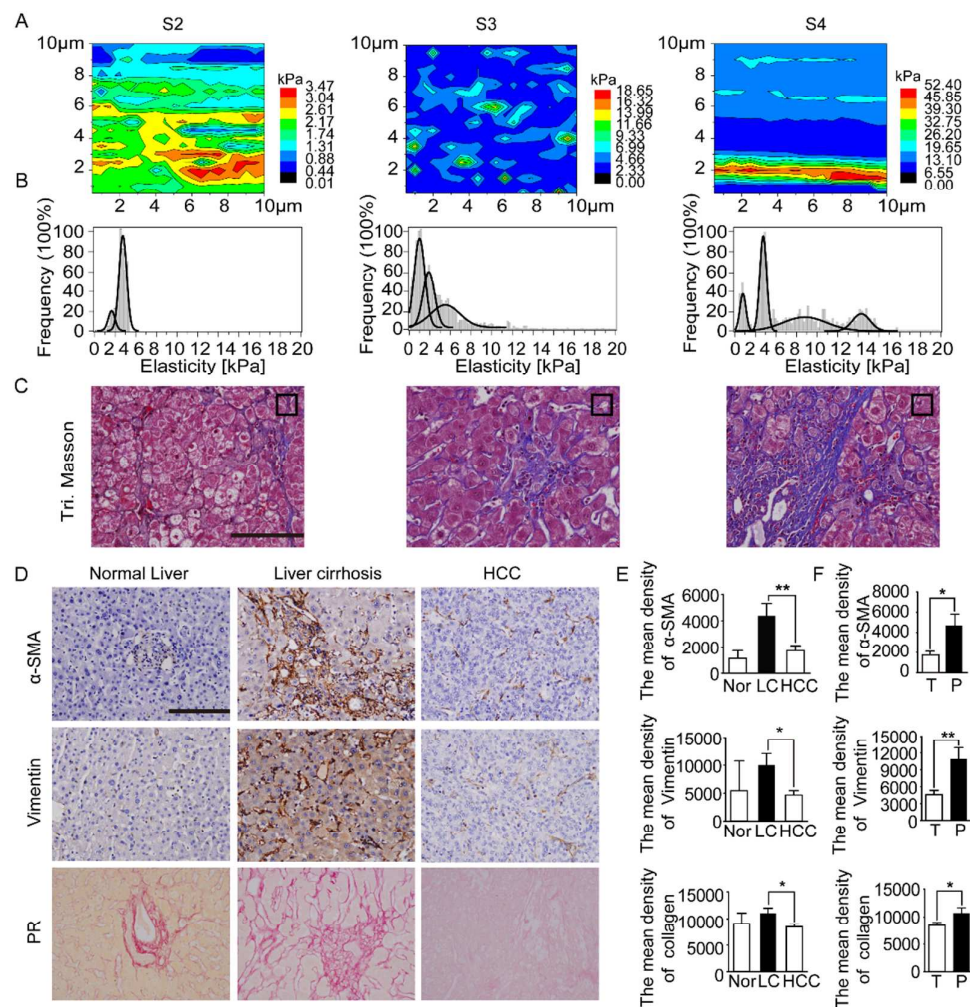
Figure 3. Increase of ECM elasticity during cirrhotic liver development. A, B and C Elasticity maps (10μm × 10μm, 100 pixels), elasticity distributions and Tri. Masson analysis of cirrhotic liver tissues at different cirrhotic stages. The high elasticity peaks become more dominant when cirrhosis gets more severe. A dark square (10 μm × 10 μm, 100 pixels) represents the size of elasticity map in Tri. Masson staining. Scalebar: applies to all images, 50 μm. D, IHC showed that α-SMA, and vimentin and collagen were expressed at high level in the cirrhotic liver tissues (LC) than the normal (Nor) and the HCC tissues. The levels of collagen stained by PR followed the same trend. Scalebar: applies to all images, 50 μm. E, Quantitative analysis of the images shown in Fig. 4D revealed that the expression level of α-SMA, vimentin and collagen in cirrhotic liver were significantly higher than that that in the normal and the HCC tissues. F, Student's t test showed that the mean density of α-SMA, Vimentin and Collagen in paratumor (P) were statistically higher than that in tumor (T). * P< 0.05; ** P< 0.01.

Upshift of the HEP during cirrhotic liver development

Tissue elasticity plays an important role in tumor metastasis and progression [38-40]. Many components of the fibrillar ECM, including collagen I, III and IV, are synthesized by fibroblasts[41] and are thought to contribute to cancer-associated stiffening[42]. The ECM is abundant, especially in cirrhotic liver tissues. We found that the HEPs of cirrhotic liver tissues were directly correlated with the stage of the cirrhotic liver; therefore, the HEP may serve as an indicator to estimate carcinogenic potential. Fibrosis of the cirrhotic liver was classified into 5 groups: S0, no fibrosis; S1, portal fibrosis without septa; S2, periportal fibrosis and few septa; S3, septal fibrosis; and S4, cirrhosis[29]. As shown in Fig. 3A-B and Fig. S14D, the results demonstrated that S2, S3 and S4 showed distinct nanomechanical properties. The increase in ECM rigidity was in accord with the development of a cirrhotic liver. Images of tissues specifically stained for collagen (Tr. Masson staining) indicated that the HEP values were directly correlated

with the amount of ECM (Fig. 3C). Analyzed areas that were rich in ECM exhibited more HEPs with broad distributions. In contrast, the elasticity distribution was close to that of normal tissues in areas with less-abundant ECM. However, the amount of ECM in the tissue was not directly related to cancer. Immunohistochemistry (IHC) showed that α-SMA and vimentin were strongly expressed in cirrhotic liver tissues but were expressed at lower levels in normal and cancerous tissues (Fig. 3D, top and middle). Therefore, it is not possible to use HEPs as direct indicators for cancer. This idea was corroborated by further quantitative analysis of the expression levels of α-SMA, vimentin and collagen in 43 pairs of tissue specimens obtained from patients diagnosed with HCC. Student's t-test clearly showed significant differences between the expression levels of these biomarkers in neoplasms and paraneoplasms (Fig. 3F). However, there was no significant difference between normal and cirrhotic liver tissues (Fig. 3E). Therefore, the amount and elasticity of the ECM cannot serve as a signature of cancer

malignancy despite the fact that ECM elasticity may affect the metastasis and progression of cancer cells.

**The mechanism behind the LSP downshift**

Because we observed that the LSP downshift could serve as a nanomechanical fingerprint of liver cancer, we decided to investigate the mechanism underlying this change. To do so, we investigated the nanomechanical properties of different types of HCC cell lines. Previous mechanical measurements in cells cultured in vitro indicated that cells with higher metastatic potential had lower elastic moduli[43], suggesting that the deformability of cancer cells was associated with tumor invasion and metastasis. The HCC cell lines we tested were divided into 3 classes based on their invasive and metastatic potential: normal (L02), low metastatic potential (SMMC7721 and Huh7) and high metastatic potential (MHCC97L, MHCC97H, and HCCLM3). IT-AFM analysis revealed that the elasticity values of the HCC cell lines were between 0.22 and 1.02 kPa (Table S2). The elasticity for cells with high metastatic potential showed a sharp peak with a narrow distribution, while the elasticity for cell lines with low metastatic potential exhibited a single broad peak (Fig. 4A). There was no difference between the L02 cell line and the low-metastatic-potential cell lines (Fig. 4B). Consistent with previous findings, the nanomechanical properties of the low- and high-metastatic-potential cells were significantly different[44]. The invasive and metastatic abilities of the HCC cells increased with decreasing rigidity. Interestingly, such changes were in agreement with the changes in the LEP of liver

tissues as they moved towards carcinogenesis, further indicating that the downshift in LEP is indeed an important nanomechanical signature of neoplasia.

As HCC cells with high deformability are prone to metastasis and vascular invasion, we investigated whether tumor tissues with softer tumor cells indeed possessed high metastatic ability. Pathological diagnosis revealed that microscopic vascular invasion was present in 6 out of 15 patients (including patients with recurrent liver cancer). Interestingly, the values of the LSP were significantly different between the microscopic vascular invasion group (0.41 ± 0.07 kPa) and the non-invasion group (0.66 ± 0.08 kPa) (Fig. 4C, P=0.0487).

The RhoC-mDia1 pathway is responsible for decreased cell elasticity

Next, we investigated the molecular origin of the downshift of the LEP in liver cancer tissues and in HCC cells. It has been reported that cytoskeletal architecture can significantly influence cell mechanics and disease state[12]. Generally, cytoskeletal responses to cell signaling are mediated by the Rho family of GTPases. ROCK1 and mDia1 are two major effectors of the Rho family that may be involved in the remodeling of microtubules and F-actin[45]. We hypothesized that the expression level of mDia1 or ROCK1 may directly correlate with the change in LEP in liver tissues. Thus, we examined mDia1 and ROCK1 expression in a set of different liver tissues that displayed gradually increased elasticity. Indeed, our IHC results confirmed that mDia1 expression was positively correlated with
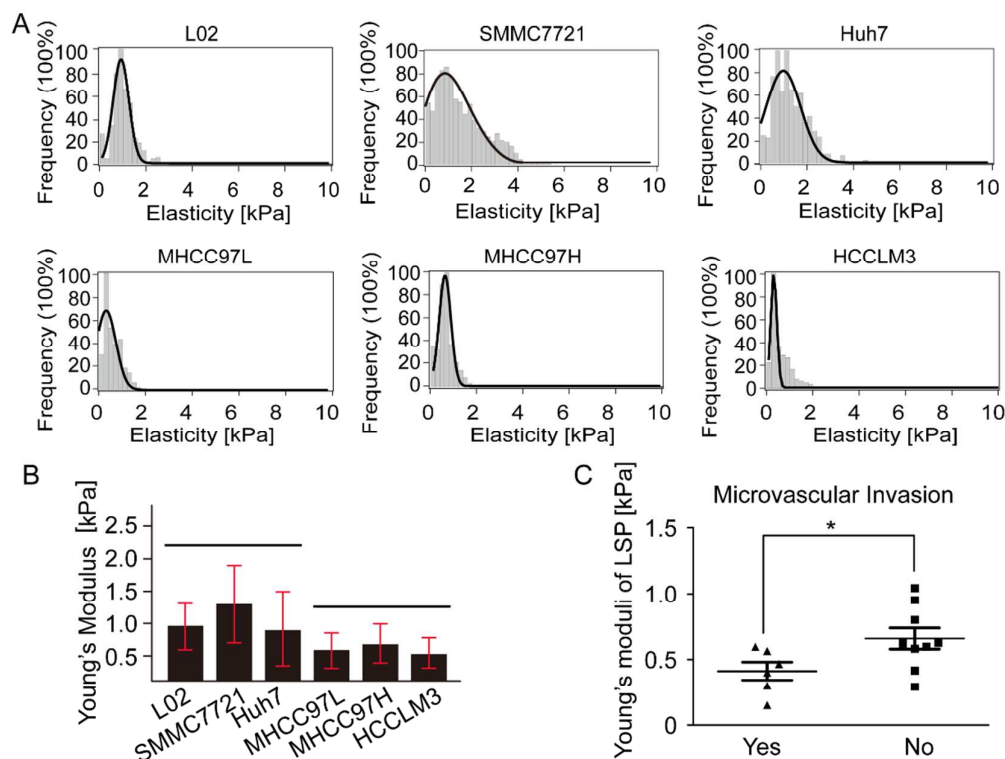
Journal Name

ARTICLE

Figure 4. Downshift of LEP in cancer tissue is correlated with the increase of metastasis of different cancer cells. A, The elasticity histograms of different HCC cell lines. B, The deformability of HCC cell lines changed with the increase of invasiveness and metastatic potential. C, In HCC tissues, the Young's moduli of the LEP is correlated with the microvascular invasion ability, Student's t test, P=0.048.

the elasticity of the corresponding specimens (Fig. 5A, Fig. S9), whereas ROCK1 expression did not follow the same trend (Fig. S10). Furthermore, we observed increased F-actin expression levels in stiffer tissues (Fig. 5A).

To identify the link between the mDia1 pathway and the mechanical properties of liver cancer cells, we knocked down the expression of mDia1 in two representative HCC cell lines (SMMC7721 and Huh7) using RNA interference. As shown in Fig. 5B, both SMMC7721 and Huh7 cells treated with mDia1 siRNA (SMMC7721 simDia1 and Huh7 simDia1) showed a similar downregulation of mDia1 at the mRNA and protein levels. IT-AFM revealed that the Young's moduli of the knockdown cell lines were significantly decreased (Fig. 5C), in sharp contrast to the control group. Moreover, F-actin staining demonstrated that the cytoskeleton was significantly altered in the SMMC7721 simDia1 and Huh7 simDia1 treatment lines (Fig. 5D). Together, these data indicate that mDia1 is crucial for the changes in the mechanical properties observed for the liver cancer cell lines.

Moreover, we found that mDia1 siRNA could suppress the growth of the SMMC7721 and Huh7 cell lines (p < 0.05), suggesting that mDia1 is also important for the growth of HCC cell lines (Fig. 5E). We also explored whether mDia1 was associated with altered cell migration. In vitro migration assays showed that the number of migrating SMMC7721 simDia1 or Huh7 simDia1 cells was significantly higher than the number of cells in the SMMC7721 and Huh7 control groups (Fig. 5F, p < 0.001), suggesting that decreased mDia1 expression levels can promote cancer cell migration. Next, we investigated the mRNA and protein expression levels of other proteins related to the mDia1 pathway, including RhoA, RhoB, RhoC, ROCK1 and mDia1. Interestingly, the expression levels of RhoC and its downstream effector ROCK1 were significantly upregulated following treatment with mDia1 siRNA (Fig. 5G, p < 0.05), while the expression levels of RhoA and RhoB did not change. This result indicated that RhoC is the activator of both mDia1 and ROCK1 and that inhibition of the RhoC-mDia1 pathway can activate the RhoC-ROCK1 pathway. The RhoC-ROCK1 pathway has been reported to facilitate liver cancer cell migration and invasion[46]. Thus, the changes in the mechanical properties of liver cancer cells may also promote cancer invasion and metastasis by indirectly upregulating this pathway.

Finally, we sought to identify other phosphorylation-based signaling pathways related to the RhoC-mDia1 pathway that were involved in the cell softening phenotype. To do so, we analyzed the phosphorylation states of key signaling proteins, including Akt (PI3K-Akt pathway), ERK1/2 (ERK1/2 pathway), JNK (JNK pathway) and STAT3 (JAK/STAT pathway). As shown in Fig. 5H, mDia1 knockdown led to a significant increase in the phosphorylation level of ERK1/2 but did not affect the phosphorylation of Akt, JNK or STAT3 in the SMMC7721 simDia1 and Huh7 simDia1 cell lines (Fig. S11). ERK signaling can be activated by numerous extracellular signals, some of which are directly relevant to cancer[47]. Therefore, the softening of liver cancer cells is directly correlated with the upregulation of mDia1 and the deregulation of the ERK1/2 pathway, thereby ultimately promoting cancer progression.

Lower mDia1 expression is correlated with poorer prognosis

We analyzed the clinical significance of mDia1 expression using a tissue microarray composed of primary tumors from 751 HCC patients. Representative cases of IHC staining are shown in Fig. 5I. By the last follow-up date in November 2012, 55.0% (413/751) of the patients had suffered a recurrence, while 38.5% (289/751) had died. The 1-, 3-, and 5-year overall survival rates were 89.1%, 70.2%, and 61.5%, respectively. The 1-, 3-, and 5-year cumulative recurrence rates were 26.0%, 45.5%, and 55.0%, respectively. Importantly, the 1-, 3-, and 5-year survival rates of the mDia1[High] patients were significantly higher than the survival rates of patients in the mDia1[Low] group (89.1% versus 89.1%, 72.8% versus 63.8%, and 64.7% versus 53.8%, high versus low, respectively) (Fig. 5I, right top); there was no significant difference between their cumulative recurrence rates (Fig. 5I, right bottom). Univariate analysis of patient survival was performed based on clinicopathological parameters. mDia1 was an independent risk factor for overall survival (OS), while ALB, γ-GT, AFP, tumor number, tumor size and microvascular invasion were independent predictors for OS (Table S3). These data further indicated that the elasticity of cancer cells, mediated by an mDia1-related pathway, plays an important role in cancer progression and death. However, more tissue samples from HCC patients should be measured using IT-AFM to validate this conclusion.
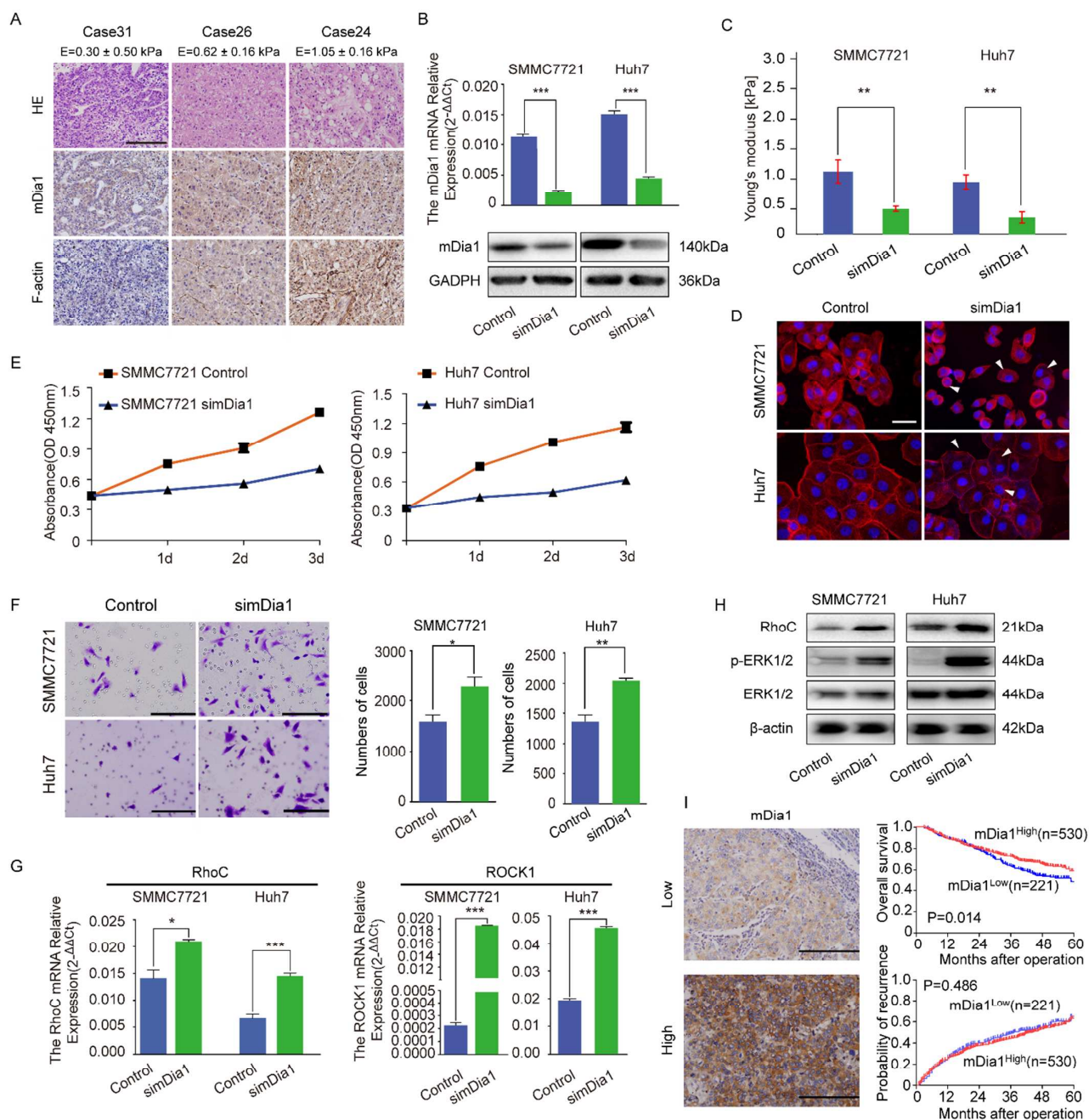
Figure 5. RhoC-mDia1 pathway is responsible for the decrease of liver cancer cell elasticity. A, mDia1 and F-actin expression levels were in line with the tissue elasticity, as revealed by the immunohistochemical staining. Scalebar: 50 μm. B, mDia1 expression in SMMC7721 and Huh7 was altered by mDia1 siRNA and verified by qRT-PCR and western blot. C, The Young's moduli of SMMC7721 and Huh7 cells were decreased obviously when treated with mDia1 siRNA. D, F-actin staining of SMMC7721 and Huh7 cells with (simDia1) and without (Control) mDia1 siRNA. Arrows highlight the cells exhibiting F-actin remodeling upon the mDia1 siRNA treatment. Scalebar: 20 μm. E, The growth of SMMC7721 and Huh7 cell lines was inhibited by the mDia1 siRNA. F, The migration of cancer cells was measured by the transwell assay. Scalebar: 50 μm. G, RhoC and ROCK1 were upregulated in SMMC7721 and Huh7 treated with mDia1 siRNA and was confirmed by qRT-PCR. H, Downregulation of mDia1 induced the overexpression of RhoC and the phosphorylation of ERK1/2 in both SMMC7721 and Huh7 cells, as verified by western blot. I, Kaplan–Meier analysis of OS and TTR for the mDia1 expression level in tissue samples from 751 HCC patients. IHC showed representative images corresponding to the low and high expression levels of mDia1 in HCC. Scalebar: 50 μm.

Discussion

A growing number of studies have reported that biomechanics play a crucial role in many aspects of tumor development and especially in metastasis[3]. However, the majority of these studies have focused on ECM elasticity[4, 38, 42, 48-50], while few of them have analyzed the nanomechanics of tumor tissues. By measuring the mechanical properties of HCC tissues and cells, we demonstrated that tumorigenic areas were softer compared with their counterparts. Moreover, we found that different stages of HCC, including recurrent HCC, had specific

mechanical signatures. We showed that the LEP in the mechanical profile of HCC tissues was directly correlated with the nanomechanics of cancer cells and could be used as a biophysical signal for cancer diagnosis. Additionally, tumor tissues with lower elasticity were prone to microvascular invasion. The expression levels of mDia1 decreased along with increased deformability in the HCC cell lines. Furthermore, we found that mDia1 depletion led to decreased tumor cell rigidity, activation of the RhoC-ROCK1 pathway and upregulation of the ERK1/2 signaling pathway, thereby ultimately promoting cancer growth and metastasis. This finding was corroborated by clinical data.

Typically the studies on the whole tissue samples show that the cancer tissues are considerably more rigid than the surrounding tissues due to the increase of matrix deposition and crosslinking during cancer progression. However, single cell measurements reveal that cancer cells are softer than the healthy ones. The advantageous of IT-AFM is that it can resolve the mechanical properties of local area in the tissue and distinguish the mechanical properties of the cells and ECM in the same tissue. Therefore, we observed the downshift of the Young's moduli of the LEP, corresponding to the elasticity of the cancer cells in the tissues during cancer progression. For Liver cirrhosis sample shown in Figure 3, the axis for the distribution of Young's moduli was set between 0 and 10 kPa to emphasize the changes of the mechanical properties of the cell only in the tissue. However, as indicated by the elasticity map, there are quite bit spots showing elasticity higher than 10 kPa, corresponding to the elasticity of ECM.

Cancerous cells cultured in vitro have been intensively studied since AFM was first used to study bladder cancer cells in 19997. However, very few studies have focused on clinical specimens from patients[14, 51, 52] or on tumor tissues[15]. Tissue specimens from solid tumors are particularly complex and exhibit a myriad of molecular, cellular, and architectural changes. In this study, fresh live surgical liver specimens were collected and preserved in Dulbecco's Modified Eagle Medium (DMEM) with phosphatase inhibitors at 4°C. IT-AFM measurements were then taken within one day to prevent tissue degradation. Due to the high spatial resolution of this technique, we were able to resolve the mechanical properties of different components in the tumor tissues. These results were further supported by measurements of cancer cell mechanics and other biochemical studies. Our study demonstrates that IT-AFM-based nanomechanical measurements can provide unique mechanical cues for diagnosing cancer and for understanding how the mechanical properties of cells and the ECM can affect cancer metastasis and progression.

We also attempted to elucidate the molecular mechanisms underlying the changes in the mechanical properties of liver cancer tissues. The mechanical properties of cancer cells are directly associated with cytoskeletal remodeling. Janmey et al. found that actin filaments could sustain much higher stresses and withstand deformation at a much higher rate compared to other fibers in the cytoskeleton and that their concentrations determine the mechanical properties of the cell [53]. Because

the Rho GTPase family plays a key role in the formation of the actin cytoskeleton[54], we hypothesized that the changes in the mechanical properties of liver tumors are mainly associated with a Rho family-related pathway. We discovered that the expression level of mDia1, the downstream effector of RhoC, was associated with the changes in the cellular mechanical profiles. This result is consistent with findings on the function of mDia1 in the generation of linear actin filaments[55-57]. Moreover, we discovered that knockdown of the mDia1 pathway could also activate another downstream effector of RhoC (ROCK1), which is also responsible for HCC cell invasion and metastasis[58-62]. The interplay between the RhoC-mDia1 and RhoC-ROCK1 pathways in liver tumor metastasis and invasion warrants further investigation. Clinical data showed that HCC patients bearing tumors with low mDia1 expression levels had a poorer prognosis than their counterparts, further underscoring the importance of mDia1 in cancer mechanics, invasion and metastasis.

Conclusion

In summary, our study provides the first direct measurement of the nanomechanical properties of liver cancer tissues. Owing to the high spatial resolution of the IT-AFM technique, we could directly resolve the mechanics of cancer cells and the ECM in the mechanical profiles of tissue samples. We discovered that the LEP of the tissue samples corresponded to the mechanical properties of the epithelial cells within the tissue; these results can be used as a unique nanomechanical fingerprint for cancer diagnosis across diverse types of liver cancer. We further showed that the changes in the nanomechanical properties of liver cancer tissues can serve as a reporter for cancer progression. To date, IT-AFM techniques are still limited to a few biophysics laboratories. Developing more user-friendly and automated assays could greatly expand the application of this technique in cancer diagnosis. Moreover, we uncovered the molecular origin of the altered nanomechanical properties of liver cancer tumors using various biochemical and cell biological techniques. We discovered that the changes in the mechanical properties of liver cancer cells were correlated with the expression level of mDia1. This finding suggests that it may be possible to regulate cancer progression and metastasis using simple mechanical perturbations of cancer tissues. However, more detailed studies are required to understand the nanomechanics of liver cancer tissues from a therapeutic point of view.

Acknowledgements

The conclusions section should come in this section at the end of the article, before the acknowledgements.

Notes and references

1. 1.D. E. Ingber, L. Dike, L. Hansen, S. Karp, H. Liley, A. Maniotis, H. McNamee, D. Mooney, G. Plopper, J. Sims and et al., *International review of cytology*, 1994, **150**, 173-224.
2. 2.D. T. Butcher, T. Alliston and V. M. Weaver, *Nature reviews. Cancer*, 2009, **9**, 108-122.
3. 3.D. Wirtz, K. Konstantopoulos and P. C. Searson, *Nature reviews. Cancer*, 2011, **11**, 512-522.
4. 4.J. G. Goetz, S. Minguet, I. Navarro-Lerida, J. J. Lazcano, R. Samaniego, E. Calvo, M. Tello, T. Osteso-Ibanez, T. Pellinen, A. Echarri, A. Cerezo, A. J. Klein-Szanto, R. Garcia, P. J. Keely, P. Sanchez-Mateos, E. Cukierman and M. A. Del Pozo, *Cell*, 2011, **146**, 148-163.
5. 5.S. A. Lelievre, V. M. Weaver, J. A. Nickerson, C. A. Larabell, A. Bhaumik, O. W. Petersen and M. J. Bissell, *Proceedings of the National Academy of Sciences of the United States of America*, 1998, **95**, 14711-14716.
6. 6.C. Rotsch, K. Jacobson and M. Radmacher, *Proceedings of the National Academy of Sciences of the United States of America*, 1999, **96**, 921-926.
7. 7.M. Lekka, P. Laidler, D. Gil, J. Lekki, Z. Stachura and A. Z. Hrynkiewicz, *European biophysics journal : EBJ*, 1999, **28**, 312-316.
8. 8.M. L. Gardel, J. H. Shin, F. C. MacKintosh, L. Mahadevan, P. Matsudaira and D. A. Weitz, *Science (New York, N.Y.)*, 2004, **304**, 1301-1305.
9. 9.C. Guilluy, L. D. Osborne, L. Van Landeghem, L. Sharek, R. Superfine, R. Garcia-Mata and K. Burridge, *Nature cell biology*, 2014, **16**, 376-381.
10. 10.R. M. Hochmuth, *Journal of biomechanics*, 2000, **33**, 15-22.
11. 11.A. Fuhrmann, J. R. Staunton, V. Nandakumar, N. Banyai, P. C. Davies and R. Ros, *Physical biology*, 2011, **8**, 015007.
12. 12.S. Suresh, *Acta biomaterialia*, 2007, **3**, 413-438.
13. 13.J. Guck, S. Schinkinger, B. Lincoln, F. Wottawah, S. Ebert, M. Romeyke, D. Lenz, H. M. Erickson, R. Ananthakrishnan, D. Mitchell, J. Kas, S. Ulvick and C. Bilby, *Biophysical journal*, 2005, **88**, 3689-3698.
14. 14.S. E. Cross, Y. S. Jin, J. Rao and J. K. Gimzewski, *Nature nanotechnology*, 2007, **2**, 780-783.
15. 15.M. Plodinec, M. Loparic, C. A. Monnier, E. C. Obermann, R. Zanetti-Dallenbach, P. Oertle, J. T. Hyotyla, U. Aebi, M. Bentires-Alj, R. Y. Lim and C. A. Schoenenberger, *Nature nanotechnology*, 2012, **7**, 757-765.
16. 16.D. E. Ingber, *Annals of medicine*, 2003, **35**, 564-577.
17. 17.C. T. Lim, E. H. Zhou and S. T. Quek, *Journal of biomechanics*, 2006, **39**, 195-216.
18. 18.A. N. Ketene, P. C. Roberts, A. A. Shea, E. M. Schmelz and M. Agah, *Integrative biology : quantitative biosciences from nano to macro*, 2012, **4**, 540-549.
19. 19.A. Hall, *Science (New York, N.Y.)*, 1998, **279**, 509-514.
20. 20.E. Sahai and C. J. Marshall, *Nature reviews. Cancer*, 2002, **2**, 133-142.
21. 21.M. Uehata, T. Ishizaki, H. Satoh, T. Ono, T. Kawahara, T. Morishita, H. Tamakawa, K. Yamagami, J. Inui, M. Maekawa and S. Narumiya, *Nature*, 1997, **389**, 990-994.
22. 22.Y. Cai, C. H. Zhou, D. Fu and X. Z. Shen, *Journal of digestive diseases*, 2012, **13**, 327-334.
23. 23.Y. F. Peng, Y. H. Shi, Z. B. Ding, A. W. Ke, C. Y. Gu, B. Hui, J. Zhou, S. J. Qiu, Z. Dai and J. Fan, *Autophagy*, 2013, **9**, 2056-2068.
24. 24.Z. B. Ding, Y. H. Shi, J. Zhou, S. J. Qiu, Y. Xu, Z. Dai, G. M. Shi, X. Y. Wang, A. W. Ke, B. Wu and J. Fan, *Cancer research*, 2008, **68**, 9167-9175.
25. 25.W. R. Liu, M. X. Tian, L. X. Yang, Y. L. Lin, L. Jin, Z. B. Ding, Y. H. Shen, Y. F. Peng, D. M. Gao, J. Zhou, S. J. Qiu, Z. Dai, R. He, J. Fan and Y. H. Shi, *Oncotarget*, 2014.
26. 26.W. R. Liu, M. X. Tian, L. Jin, L. X. Yang, Z. B. Ding, Y. H. Shen, Y. F. Peng, J. Zhou, S. J. Qiu, Z. Dai, J. Fan and Y. H. Shi, *Journal of experimental & clinical cancer research : CR*, 2014, **33**, 32.
27. 27.Y. H. Shi, W. X. Ding, J. Zhou, J. Y. He, Y. Xu, A. A. Gambotto, H. Rabinowich, J. Fan and X. M. Yin, *Hepatology*, 2008, **48**, 497-507.
28. 28.Q. Gao, S. J. Qiu, J. Fan, J. Zhou, X. Y. Wang, Y. S. Xiao, Y. Xu, Y. W. Li and Z. Y. Tang, *Journal of clinical oncology : official journal of the American Society of Clinical Oncology*, 2007, **25**, 2586-2593.
29. 29.B. K. Kim, H. S. Kim, E. J. Yoo, E. J. Oh, J. Y. Park, D. Y. Kim, S. H. Ahn, K. H. Han, S. U. Kim and Y. N. Park, *Hepatology*, 2014, DOI: 10.1002/hep.27389.
30. 30.Q. Gao, X. Y. Wang, S. J. Qiu, I. Yamato, M. Sho, Y. Nakajima, J. Zhou, B. Z. Li, Y. H. Shi, Y. S. Xiao, Y. Xu and J. Fan, *Clinical cancer research : an official journal of the American Association for Cancer Research*, 2009, **15**, 971-979.
31. 31.R. Liao, J. Sun, H. Wu, Y. Yi, J. X. Wang, H. W. He, X. Y. Cai, J. Zhou, Y. F. Cheng, J. Fan and S. J. Qiu, *Journal of experimental & clinical cancer research : CR*, 2013, **32**, 3.
32. 32.M. Lekka, D. Gil, K. Pogoda, J. Dulinska-Litewka, R. Jach, J. Gostek, O. Klymenko, S. Prauzner-Bechcicki, Z. Stachura, J. Wiltowska-Zuber, K. Okon and P. Laidler, *Archives of biochemistry and biophysics*, 2012, **518**, 151-156.
33. 33.K. Radotic, C. Roduit, J. Simonovic, P. Hornitschek, C. Fankhauser, D. Mutavdzic, G. Steinbach, G. Dietler and S. Kasas, *Biophysical journal*, 2012, **103**, 386-394.
34. 34.C. Roduit, S. Sekatski, G. Dietler, S. Catsicas, F. Lafont and S. Kasas, *Biophysical journal*, 2009, **97**, 674-677.
35. 35.P. Colombo, F. Di Blasi, S. Magrin, C. Fabiano, V. Di Marco, L. D'Amelio, F. Lojacono, G. Spinelli and A. Craxi, *Journal of hepatology*, 1991, **12**, 64-69.
36. 36.D. Schuppan and N. H. Afdhal, *Lancet*, 2008, **371**, 838-851.
37. 37.Z. Y. Tang, S. L. Ye, Y. K. Liu, L. X. Qin, H. C. Sun, Q. H. Ye, L. Wang, J. Zhou, S. J. Qiu, Y. Li, X. N. Ji, H. Liu, J. L. Xia, Z. Q. Wu, J. Fan, Z. C. Ma, X. D. Zhou, Z. Y. Lin and K. D. Liu, *Journal of cancer research and clinical oncology*, 2004, **130**, 187-196.
38. 38.J. K. Mouw, Y. Yui, L. Damiano, R. O. Bainer, J. N. Lakins, I. Acerbi, G. Ou, A. C. Wijekoon, K. R. Leventhal, P. M. Gilbert, E. S. Hwang, Y. Y. Chen and V. M. Weaver, *Nature medicine*, 2014, **20**, 360-367.
39. 39.J. Fenner, A. C. Stacer, F. Winterroth, T. D. Johnson, K. E. Luker and G. D. Luker, *Scientific reports*, 2014, **4**, 5512.
40. 40.E. L. Baker, J. Srivastava, D. Yu, R. T. Bonnecaze and M. H. Zaman, *PloS one*, 2011, **6**, e20355.
41. 41.R. Kalluri and M. Zeisberg, *Nature reviews. Cancer*, 2006, **6**, 392-401.
42. 42.K. R. Leventhal, H. Yu, L. Kass, J. N. Lakins, M. Egeblad, J. T. Erler, S. F. Fong, K. Csiszar, A. Giaccia, W. Weninger, M. Yamauchi, D. L. Gasser and V. M. Weaver, *Cell*, 2009, **139**, 891-906.
43. 43.Z. Zhou, C. Zheng, S. Li, X. Zhou, Z. Liu, Q. He, N. Zhang, A. Ngan, B. Tang and A. Wang, *Nanomedicine : nanotechnology, biology, and medicine*, 2013, DOI: 10.1016/j.nano.2013.04.001.
44. 44.V. Swaminathan, K. Mythreye, E. T. O'Brien, A. Berchuck, G. C. Blobe and R. Superfine, *Cancer research*, 2011, **71**, 5075-5080.

45 45.T. Ishizaki, Y. Morishima, M. Okamoto, T. Furuyashiki, T. Kato and S. Narumiya, *Nature cell biology*, 2001, **3**, 8-14.
46 46.K. Itoh, K. Yoshioka, H. Akedo, M. Uehata, T. Ishizaki and S. Narumiya, *Nature medicine*, 1999, **5**, 221-225.
47 47.A. S. Dhillon, S. Hagan, O. Rath and W. Kolch, *Oncogene*, 2007, **26**, 3279-3290.
48 48.D. Choquet, D. P. Felsenfeld and M. P. Sheetz, *Cell*, 1997, **88**, 39-48.
49 49.A. M. Baker, D. Bird, G. Lang, T. R. Cox and J. T. Erler, *Oncogene*, 2013, **32**, 1863-1868.
50 50.V. Seewaldt, *Nature medicine*, 2014, **20**, 332-333.
51 51.S. E. Cross, Y. S. Jin, J. Tondre, R. Wong, J. Rao and J. K. Gimzewski, *Nanotechnology*, 2008, **19**, 384003.
52 52.M. Stolz, R. Gottardi, R. Raiteri, S. Miot, I. Martin, R. Imer, U. Staufer, A. Raducanu, M. Duggelin, W. Baschong, A. U. Daniels, N. F. Friederich, A. Aszodi and U. Aebi, *Nature nanotechnology*, 2009, **4**, 186-192.
53 53.P. A. Janmey, U. Euteneuer, P. Traub and M. Schliwa, *The Journal of cell biology*, 1991, **113**, 155-160.
54 54.K. Burridge and K. Wennerberg, *Cell*, 2004, **116**, 167-179.
55 55.E. Geron, E. D. Schejter and B. Z. Shilo, *Proceedings of the National Academy of Sciences of the United States of America*, 2013, **110**, 10652-10657.
56 56.A. Jegou, M. F. Carlier and G. Romet-Lemonne, *Nature communications*, 2013, **4**, 1883.
57 57.C. Higashida, T. Kiuchi, Y. Akiba, H. Mizuno, M. Maruoka, S. Narumiya, K. Mizuno and N. Watanabe, *Nature cell biology*, 2013, **15**, 395-405.
58 58.J. G. Zhang, X. Y. Li, Y. Z. Wang, Q. D. Zhang, S. Y. Gu, X. Wu, G. H. Zhu, Q. Li and G. L. Liu, *PloS one*, 2014, **9**, e107661.
59 59.L. Xia, W. Huang, D. Tian, H. Zhu, Y. Zhang, H. Hu, D. Fan, Y. Nie and K. Wu, *Journal of hepatology*, 2012, **57**, 600-612.
60 60.P. W. Voorneveld, L. L. Kodach, R. J. Jacobs, N. Liv, A. C. Zonnevylle, J. P. Hoogenboom, I. Biemond, H. W. Verspaget, D. W. Hommes, K. de Rooij, C. J. van Noesel, H. Morreau, T. van Wezel, G. J. Offerhaus, G. R. van den Brink, M. P. Peppelenbosch, P. Ten Dijke and J. C. Hardwick, *Gastroenterology*, 2014, **147**, 196-208 e113.
61 61.D. J. McGrail, Q. M. Kieu and M. R. Dawson, *Journal of cell science*, 2014, **127**, 2621-2626.
62 62.Z. Dong, S. Fu, X. Xu, Y. Yang, L. Du, W. Li, S. Kan, Z. Li, X. Zhang, L. Wang, J. Li, H. Liu, X. Qu and C. Wang, *British journal of cancer*, 2014, **110**, 1801-1810.
63